Wind Tunnel Measurements of the NACA63-418 Airfoil LERAP Project: Tests from the Poul la Cour Tunnel

Olsen, Anders Smærup; Beckerlee, Jimmie Stig; Ildvedsen, Sigurd Brabæk; Bak, Christian

Link to article, DOI:
10.11581/DTU.00000266

Publication date:
2021

Document Version
Publisher's PDF, also known as Version of record

Danmarks Tekniske Universitet

DTU

Wind Tunnel Measurements of the NACA63-418 Airfoil LERAP Project Tests from the Poul la Cour Tunnel Classification: Confidential

DTU Wind Energy Report-I-1216

Anders S. Olsen
Jimmie Beckerlee
Sigurd Lundsgaard Ildvedsen
Christian Bak

June 9, 2021

Contents

1 Introduction

Wind tunnel measurements were carried out on a NACA63-418 airfoil in the Poul la Cour Tunnel (PLCT) at DTU Wind Energy, Risø Campus, Roskilde, Denmark.

The test were commissioned by the LERAP project with Christian Bak as the contact person.

The tests were performed from 13th July 2020 to 16th July 2020.

The tests are confidential.

This report describes the aerodynamic model and the devices that were applied (Section 2), the test program (Section 3) and the results (Section 4). The appendices describe the experimental setup (Appendix A), the measurement techniques (Appendix B), the applied corrections (Appendix C) and the pressure orifices coordinates (Appendix D).

2 Aerodynamic models and devices

2.1 The model

The airfoil section NACA63-418 was tested. The model is from the stock at DTU wind energy.

The shape and location of the pressure orifices of the airfoil is shown in Figure 1 and the coordinates are given in Appendix D. The x-axis is in the flow direction for 0^o angle-of-attack. The airfoil model is equipped with 100 pressure taps. A check of the surface quality of the airfoil model showed a good finish.

As wrap around roughness is applied, which covers the orifices around the LE of the airfoil, the lift is based on wall pressures and drag is based on wake rake measurements and it is not possible to obtain a useful moment coefficient.

The airfoil model was mounted between the two turntables in the standard arrangement with the suction side towards the South side of the wind tunnel. There is a small gap ($\approx 0.5mm$) between the ends of the wind tunnel model and the turntable plates in order not to influence the force gauges measurements.

The 100 orifices on the airfoil model is connected to two pressure scanners located outside the tunnel.

Table 1: Airfoil model dimensions.

Name	NACA63-418
Chord [m]	1.0
Span [m]	2.0
Relative thickness [%c]	18
Pivot point [x/c, y/c]	0.40,0.0

2.2 Trip / leading edge roughness configurations

Measurements were performed with artificial roughness at the leading edge to simulate leading edge roughness of a wind turbine blade. This roughness consists of a fine and rough mesh, see Figure 2. During the tests, the meshes were placed according to Table 2.

Measurements were performed on a backward facing step close to the leading edge. The step is made from plain paper (Figure 3) and placed according to Table 3.

Table 2: Mesh configurations.

Configuration name	Position SS [%c]	Position PS [%c]
Fine[1]	3.6	3.6
Rough[1]	3.6	3.6

[1] The mesh is mounted on 0.08mm tape.

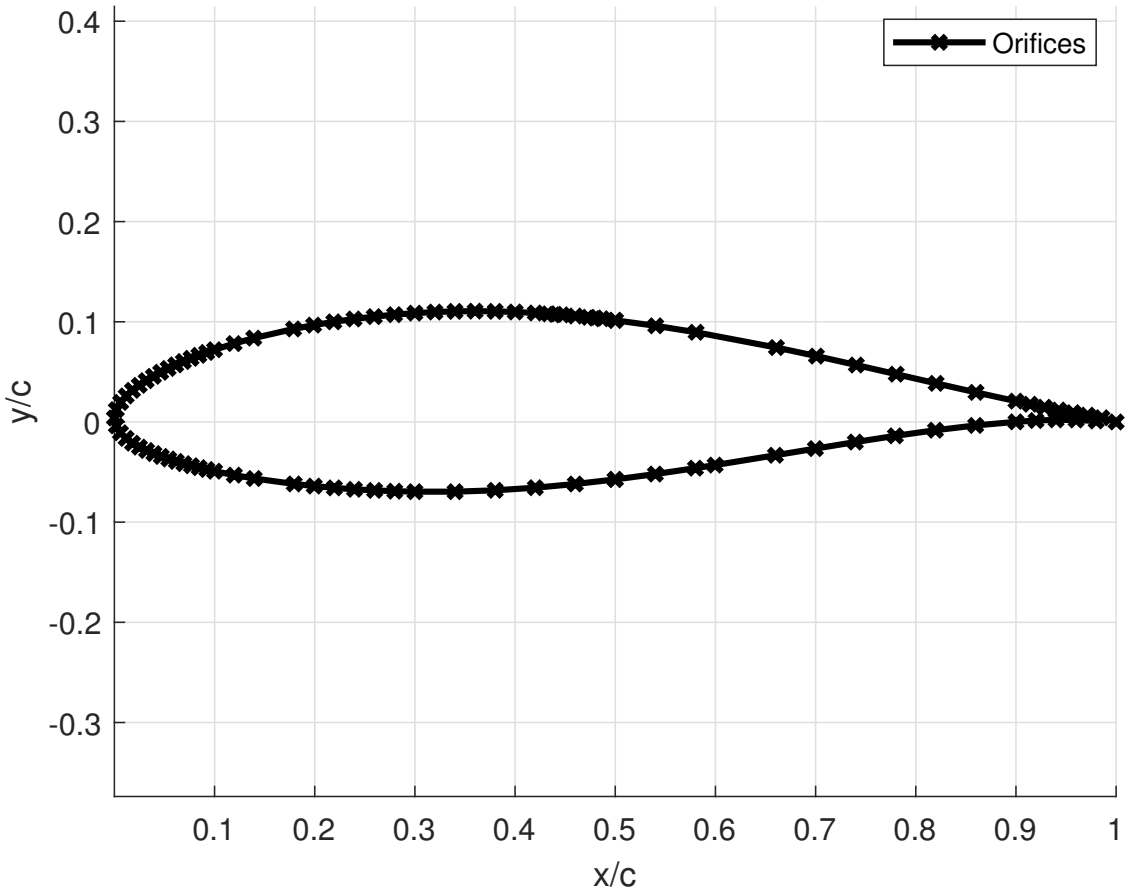

Figure 1: Orifices location on the NACA63-418.

Table 3: Step configuration.

Configuration name	Thickness[1] [mm]	Position SS [%c]	Position PS [%c]	Comment
Step1	0.8	3.6	3.6	Plain paper

[1] The paper is mounted on 0.08mm tape.

2.3 Vortex generators

Table 4 gives the tested VG configurations. From the side view, the shape of the VG is a triangle. The VG pairs are mounted on a base plate strip. The VG were mounted using double-side adhesive tape, see Figure 4.

2.4 Stall strip

Eight stall strip configurations were tested as given in Tables 5 and 6. The stall strips are 3D printed wedges that are mounted with spray glue, The stall strip is covered with tape, see Figure 5. Due to the relatively small dimensions of the stall strips the tape tends

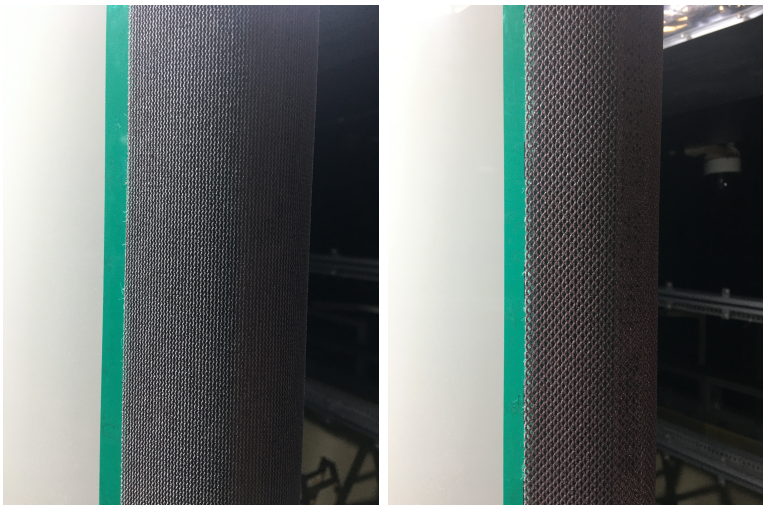

(a) (b)

Figure 2: Roughness meshes. a: Fine, b: Rough

Table 4: Vortex generator configurations.

Configuration name	Device 1
VG name	VG
Position [%c]	50
Side	SS

to smooth the kink between the airfoil surface and the stall strip wedge making the slope of the ramp lower.

Table 5: Stall strip configurations.

Configuration name	S-strip 1	S-strip 2	S-strip 3	S-strip 4
Height [mm][1]	1	2	3	1
Position [%c]	0	0	0	1
Side	SS	SS	SS	SS

[1] Height of stall strip only. The stall strip is covered by 0.08 mm tape.

Table 6: Stall strip configurations (continued).

Configuration name	S-strip 5	S-strip 6	S-strip 7	S-strip 8
Height [mm][1]	1	1	1	1
Position [%c]	2	3	1	3
Side	SS	SS	PS	PS

[1] Height of stall strip only. The stall strip is covered by 0.08 mm tape.

Figure 3: Step configuration.

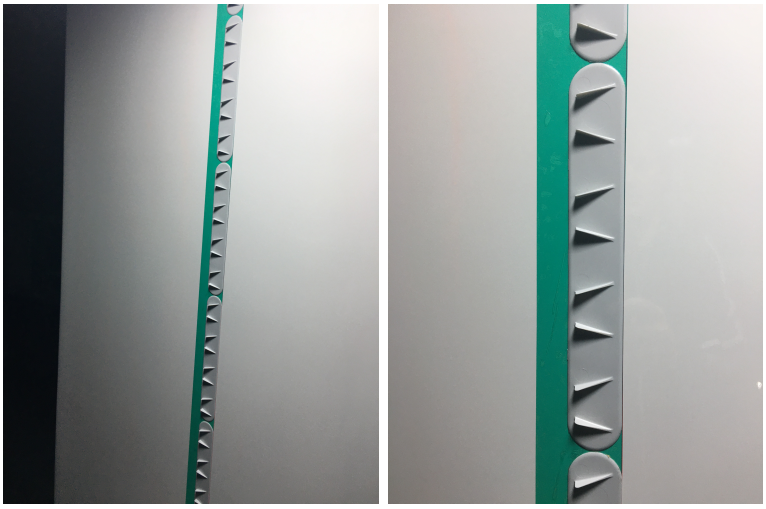

(a) (b)

Figure 4: VG configuration.

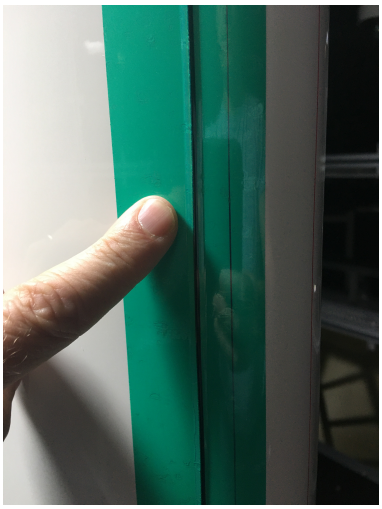

Figure 5: Stall strip configuration.

3 Test program

3.1 Test program

Tables 7 to 9 gives the test configurations including the Re and devices, with dimensions from Table 2 to Table 6.

Abbreviations used in the list:

- Re is the Reynolds number
- C_l is the lift coefficient. Here either the airfoil surface pressures (AP), the wall pressures (WP) or the force gauges (FG) can be used.
- C_d is the drag coefficient. Here either the wake rake (WR) or the force gauges (FG) can be used.
- C_m is the moment coefficient given relative to the model quarter chord ($x/c = 0.25$) from the leading edge and positive nose up. Here either the airfoil surface pressures (AP) or the force gauges (FG) can be used.
- Trip is the way that the flow is influenced to change transition characteristics. The tripping can be done by roughness meshes, steps, or stall strips.
- Devices are the aerodynamic devices such as vortex generators (VG).

Table 7: Test program for the clean polars

Meas. series #	Re	C_l	C_d	C_m	Trip[1]	Devices[2]
21	3E6	WP	WR	n/a	Clean	n/a
23	3E6	WP	WR	n/a	Clean	n/a
24	3E6	WP	WR	n/a	Clean	n/a
27	3E6	WP	WR	n/a	Clean	n/a
29	5E6	WP	WR	n/a	Clean	n/a
31	7E6	WP	WR	n/a	Clean	n/a
74	3E6	WP	WR	n/a	Clean	n/a
75	5E6	WP	WR	n/a	Clean	n/a
76	7E6	WP	WR	n/a	Clean	n/a
77[3]	3E6	WP	WR	n/a	Clean	n/a
78	5E6	WP	WR	n/a	Clean	n/a
85	5E6	WP	WR	n/a	Clean	n/a
91	5E6	WP	WR	n/a	Clean	n/a

[1] See Tables 2 to 6.
[2] See Table 4.
[3] New tape between leading edge and body of airfoil.

Table 8: Test program for the tripped polars and VG configurations.

Meas. series #	Re	C_l	C_d	C_m	Trip[1]	Devices[2]
51	5E6	WP	WR	n/a	Rough	n/a
53	5E6	WP	WR	n/a	Rough	n/a
55	5E6	WP	WR	n/a	Fine	n/a
56	3E6	WP	WR	n/a	Fine	n/a
58	7E6	WP	WR	n/a	Fine	n/a
60	5E6	WP	WR	n/a	Step1	n/a
79	5E6	WP	WR	n/a	Step1	n/a
82	3E6	WP	WR	n/a	Step1	n/a
83	5E6	WP	WR	n/a	Step1	n/a
62	5E6	WP	WR	n/a	Clean	Device 1
66	5E6	WP	WR	n/a	Rough	Device 1
68	5E6	WP	WR	n/a	Fine	Device 1
64	5E6	WP	WR	n/a	S-strip 1	Device 1
70	5E6	WP	WR	n/a	S-strip 1	Device 1

[1] See Tables 2 to 6.
[2] See Table 4.

Table 9: Test program for the stall strip configurations.

Meas. series #	Re	C_l	C_d	C_m	Trip[1]	Devices[2]
34	5E6	WP	WR	n/a	S-strip 3	n/a
37	5E6	WP	WR	n/a	S-strip 2	n/a
39	5E6	WP	WR	n/a	S-strip 1	n/a
72	5E6	WP	WR	n/a	S-strip 1	n/a
86	5E6	WP	WR	n/a	S-strip 1	n/a
87[3]	5E6	WP	WR	n/a	S-strip 1	n/a
41	5E6	WP	WR	n/a	S-strip 4	n/a
43	5E6	WP	WR	n/a	S-strip 5	n/a
45	5E6	WP	WR	n/a	S-strip 6	n/a
47	5E6	WP	WR	n/a	S-strip 7	n/a
88[4]	5E6	WP	WR	n/a	S-strip 7	n/a
90	5E6	WP	WR	n/a	S-strip 7	n/a
49	5E6	WP	WR	n/a	S-strip 8	n/a

[1] See Tables 2 to 6.
[2] See Table 4.
[3] New tape between leading edge and body of airfoil.
[4] Some glue left on LE.

4 Results

The following sections show figures with the measured data for the different configurations.

4.1 Clean

Figures 6 to 8 show the corrected C_l from the wall pressures and the corrected C_d from the wake rake for the clean configurations at different Reynold's numbers.

In the stalled regions the wake deficit is too large to be captured by the wake rake, hence the C_d-values are set to zero.

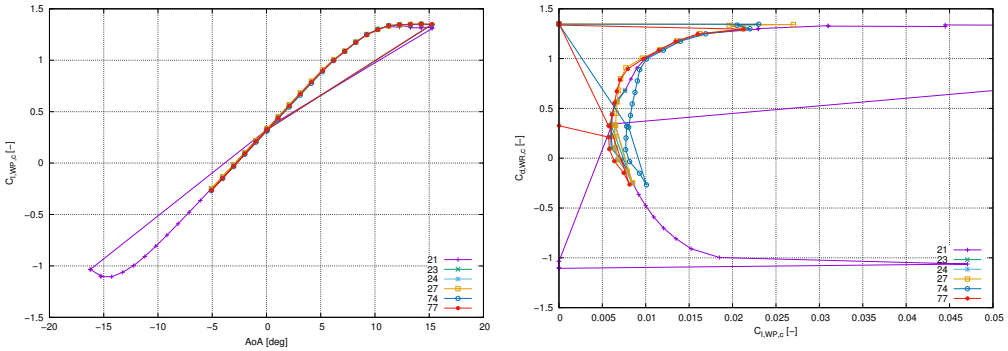

(a) (b)

Figure 6: Clean configurations. Re=3E6.

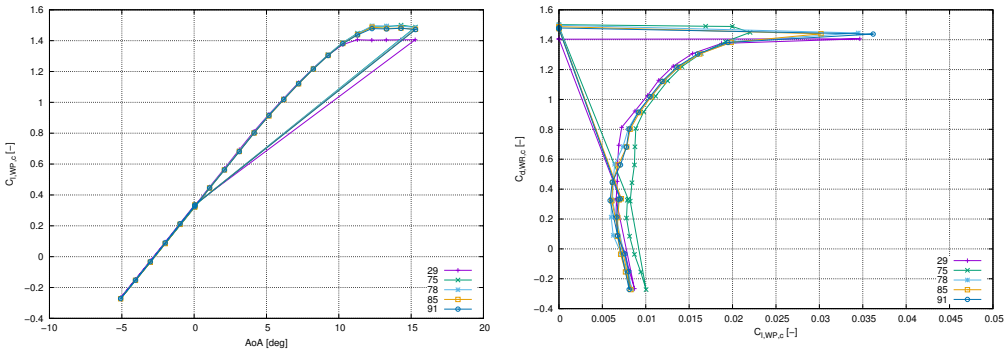

(a) (b)

Figure 7: Clean configurations. Re=5E6.

4.2 Tripped

Figures 9 to 11 show the corrected C_l from the wall pressures and the corrected C_d from the wake rake for the roughness mesh configurations at different Reynold's numbers.

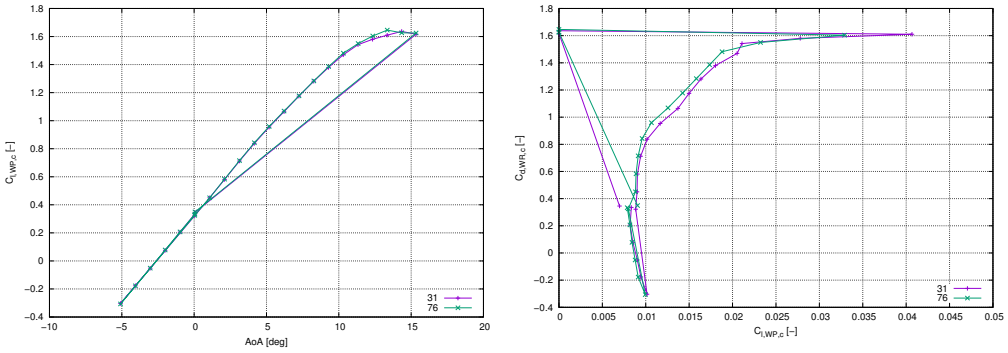

(a) (b)

Figure 8: Clean configurations. Re=7E6.

Figures 12 to 13 show the corrected C_l from the wall pressures and the corrected C_d from the wake rake for the step configurations at different Reynold's numbers.

In the stalled regions the wake deficit is too large to be captured by the wake rake, hence the C_d-values are set to zero.

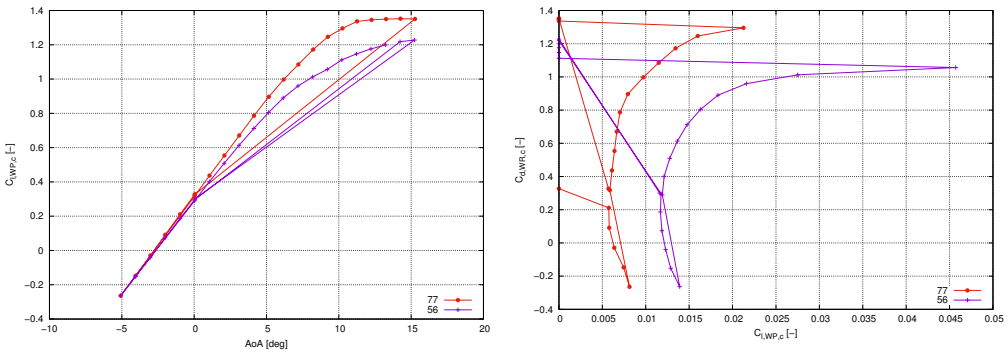

(a) (b)

Figure 9: Fine mesh. Re=3E6.

4.3 VGs

Figure 14 shows the corrected C_l from the wall pressures and the corrected C_d from the wake rake for the VG configurations at a Reynold's numbers of 5E6.

In the stalled regions the wake deficit is too large to be captured by the wake rake, hence the C_d-values are set to zero.

4.4 Stall strip

Figure 15 shows the corrected C_l from the wall pressures and the corrected C_d from the wake rake for the stall strip configurations with varying height at a Reynold's number of

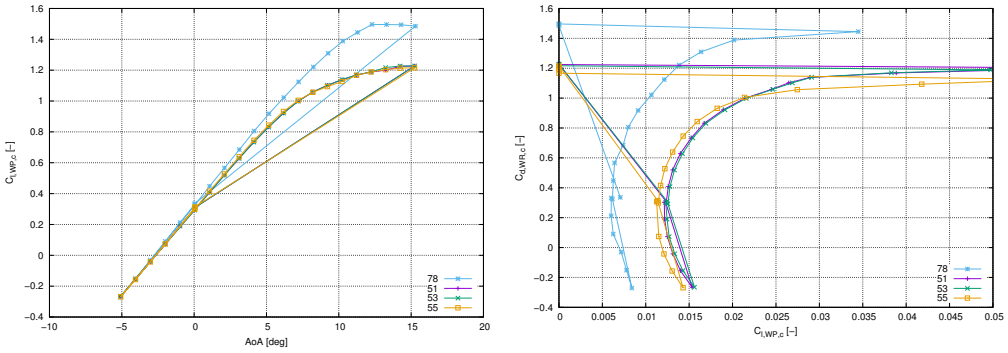

(a) (b)

Figure 10: Roughness meshes. Re=5E6.

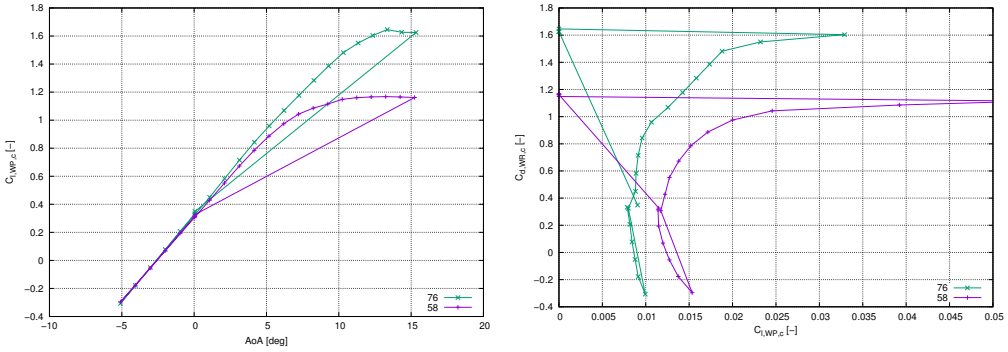

(a) (b)

Figure 11: Fine mesh. Re=7E6.

5E6.

Figure 16 shows the corrected C_l from the wall pressures and the corrected C_d from the wake rake for the stall strip configurations with varying suction side positions at a Reynold's number of 5E6.

Figure 17 shows the corrected C_l from the wall pressures and the corrected C_d from the wake rake for the stall strip configurations with varying pressure side positions at a Reynold's number of 5E6.

In the stalled regions the wake deficit is too large to be captured by the wake rake, hence the C_d-values are set to zero.

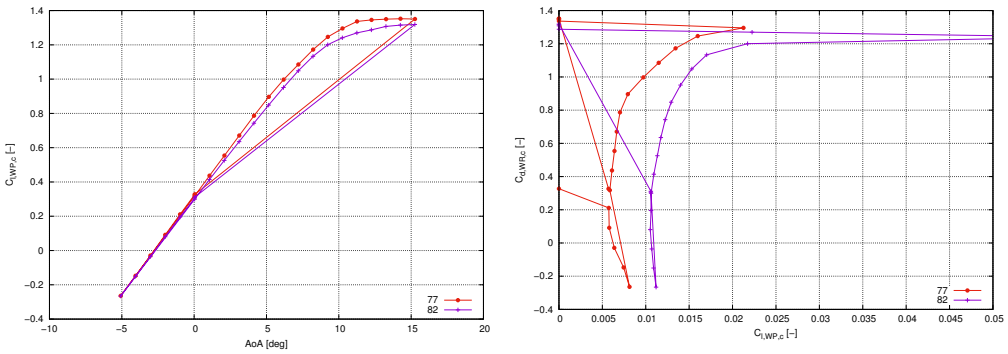

(a) (b)

Figure 12: Step configuration. Re=3E6.

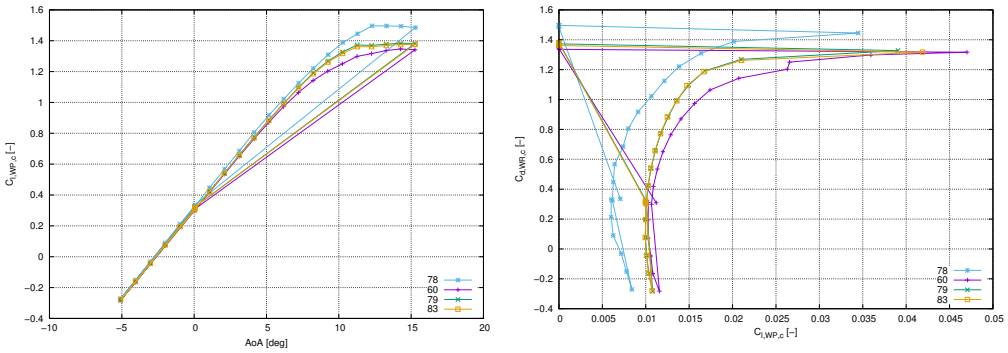

(a) (b)

Figure 13: Step configurations. Re=5E6.

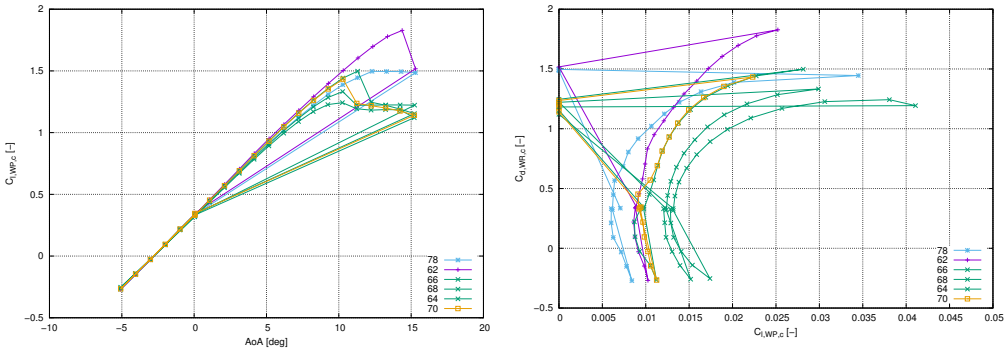

(a) (b)

Figure 14: VG configurations. Re=5E6.

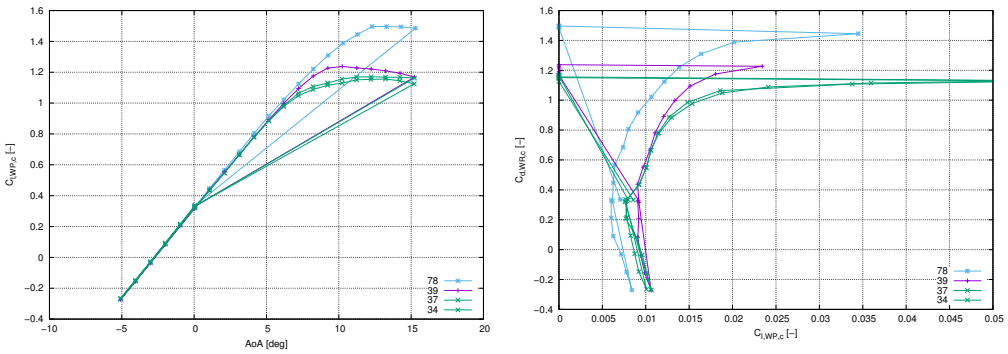

(a) (b)

Figure 15: Stall strip configurations with varying heights. Re=5E6

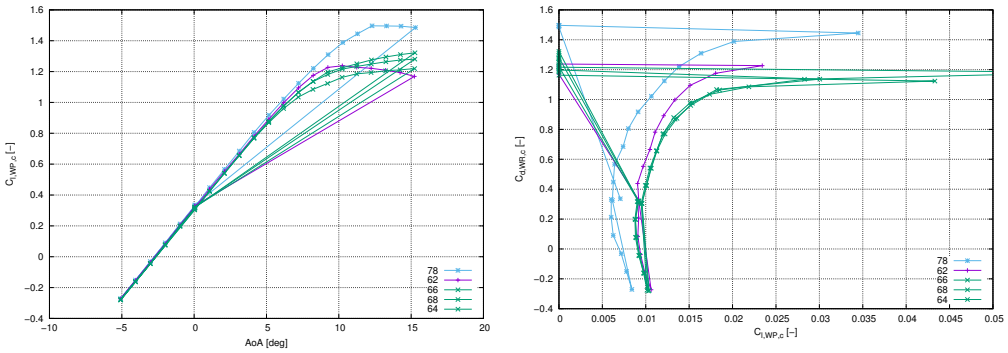

(a) (b)

Figure 16: Stall strip configurations with varying suction side positions. Re=5E6

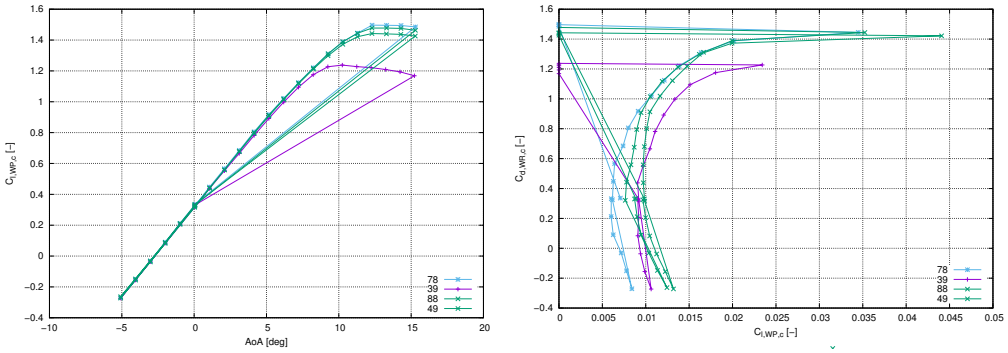

(a) (b)

Figure 17: Stall strip configurations with varying pressure side positions. Re=5E6

Appendix A Experimental setup

A.1 The wind tunnel

The PLCT is a closed return tunnel with a closed test section; see Figure A. 1.

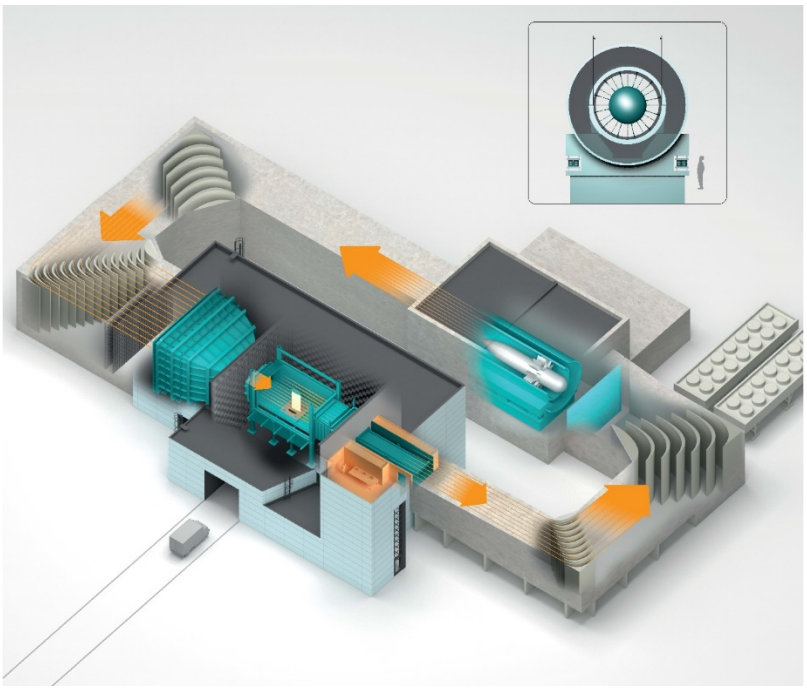

Figure A. 1. Sketch of the Poul la Cour Tunnel (PLCT).

The rectangular test section has the dimensions of height, H=2.000m and width, W=3.000m and length, L=9.000m. A 2D airfoil model spans from floor to ceiling, i.e. 2.000m. The effective contraction ratio of 9 and the system of screens and Honeycomb results in a low turbulence level of $Tu < 0.1\%$ for a frequency range of 10–5000 Hz and a flow velocity of 50 m/s.

The walls of the test section are exchangeable between aerodynamic hard walls and aeroacoustic Kevlar walls. The walls are 6 m long and cover the part of the test section that begins 1 m downstream of the contraction.

The turntable diameters are 1.355m with a 0.5m x 1.25m hatch with rounded corners. The center of the turntables are 4 m downstream of the contraction.

Appendix B Measurement techniques

Figure B. 1 shows a schematic view of the test section.

B.1 Sensors

The test section and the model is equipped with a number of sensors:

- 6 ScaniValve pressure scanners with 64 channels each and a sensitivity between 1 kPa (4 inch H2O) and 69 kPa (10 PSI). They are connected to the model orifices, the wall pressure orifices and the wake rake total and static pressure tubes
- 1 temperature sensor at the inlet of the contraction
- 1 relative humidity sensor at the inlet of the contraction
- 1 pitot tube (for static and total pressures) at the inlet of the test section
- 1 differential pressure transducer measuring the pressure difference over the contraction
- 1 temperature sensor in the anechoic room
- 1 relative humidity sensor in the anechoic room
- 1 atmospheric pressure sensor in the anechoic room
- 2 angle-of-attack encoders at the turntables
- 2 two-component force gauges in the lower turntable
- 2 encoders for the position of the wake rake in horizontal and vertical direction
- 84 microphones placed in a Bruel & Kjaer microphone array, pointing towards the model in the test section and measuring the noise, when Kevlar walls are mounted.

B.2 DAQ System

The data acquisition (DAQ) system is based upon cRIO from National Instruments and a DTU in-house made LabView program.

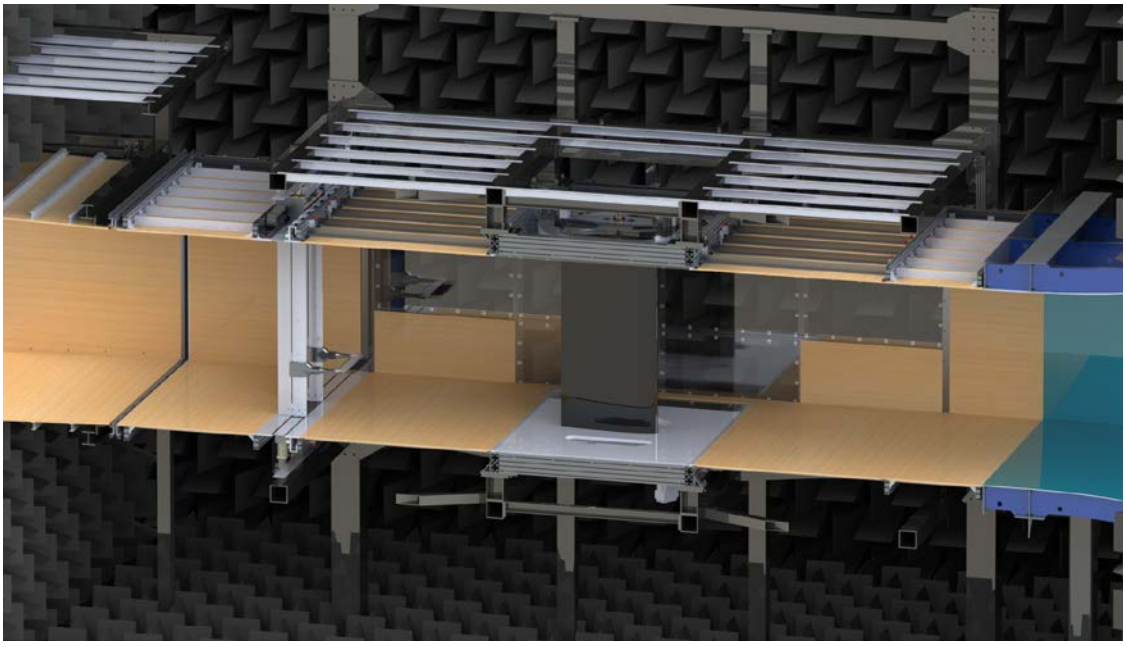

Figure B. 1: Schematic view of the test section with an airfoil model and the wake rake.

B.3 Lift measurement

The PLCT offers up to three different methods for measuring the lift force: from model surface pressures, from wall pressures and from a force balance.

The present study reports the model surface pressures only.

B.3.1 Model surface pressures

The pressures measured from surface pressure taps in the model surface are integrated to determine the lift force.

The lift force determined by the surface pressures is based on a relatively narrow spanwise extend of the pressure tabs (the pressure band) and therefore it is a local value in contrast to the lift determined by the wall pressures and force gauges. The two last methods are closer to an integrated value of the force on the entire span of the model. Hence, differences in the predicted lift by the different methods are expected. Which method that predicts the largest maximum / minimum lift depends on the location of the surface pressure band relative to the three dimensional stall cells occurring once the flow starts to separate at the trailing edge.

B.3.2 Wall pressures

Pressures are measured on two streamwise bands on each sidewall. The bands are 0.727m and 1.267m from the floor. The lower bands are connected to 48 pressure sensors and the upper bands are connected to 16 sensors.

Subtracting the pressures from the matching bands on each sidewall and integrate gives the lift force. Corrections for the missing tail part of the wall pressures as described in Althaus (2019) is applied.

Thus, two measurements of the lift force from either the top or the bottom band are obtained.

B.3.3 Force balance

Each of the two turntables have two force gauges installed (at the moment only the two at the floor is mounted). Each gauge measure the normal and tangential force components in the profile coordinate system. Through the angle of attack, the two measured force components are transferred to the lift (perpendicular to the onset flow) and drag (parallel to the onset flow) forces. In the mounting system for the model, the force gauges fully supports the model, so all forces applied on the model are transferred to the gauges. In order for the gauges to measure accurately there needs to be a small gap (~0.5mm) between the turntables and the model.

B.4 Drag measurement

The PLCT offers up to three different methods for measuring the drag force: from model surface pressures, from the wake rake and from a force balance.

The present study reports the wake rake drag for a few cases only and the surface pressure drag in all cases.

B.4.1 Model surface pressures

The integrated surface pressures also gives the drag force, however without the skin friction part. Therefore, this drag is usually lower than determined by the wake rake for attached flow. If

the distribution of the pressure taps/orifices on the model is not resolving the pressures sufficiently well the pressure drag can be higher.

For separated flow, the skin friction part is relatively low and often the wake deficit is too wide to measure by the wake rake so in this case the pressure drag is often used and is a good measure of the total (skin friction + pressure) drag.

B.4.2 Wake rake

The wake rake consists of 90 tubes measuring the total pressure and 6 Pitot tubes measuring both the static and total pressure spanning 0.695m. The spacing between the tubes is 5mm at the centre 0.395m and increasing gradually to a distance of 30mm on the outer part. It is placed 2.62m downstream of the turntable centre. It traverses a cross section of +/-0.85 m in the horizontal direction and from 0.3m to 1.7m in the vertical direction.

Based on these pressure measurements the velocity deficit behind the model can be determined and the drag force can be determined according to Jones (1936).

B.4.3 Force balance

As it is the case for measuring the lift force with the turntable, also the drag force can be measured with the force gauges in the turntables. However, there is a bigger uncertainty for the drag measurement, which should be taken into account when interpreting the measurements. The uncertainties, are minimized by conducting a “zero run” before each polar. The zero run is an angle sweep from -25 deg to +25 deg in steps of 5 deg with no wind force. This quantifies the forces from the unavoidable small misalignments in the system and they are subtracted during the analysis.
Again, no sealing between the model and the turntables gives the best results.

B.5 Pitching moment

The PLCT offers up to two different methods for measuring the pitching moment: from model surface pressures and from a force balance.

The present study reports the moment from the model surface pressures only.

B.5.1 Model surface pressures

The integrated surface pressures also gives the pitch moment. Usually it is given relative to the model quarter chord (x/c = 0.25) from the leading edge and positive nose up.

B.5.2 Force balance

As it is the case for measuring the lift force and the drag force with the turntable, also the pitch moment can be measured with the force gauges in the turntables. In this case no sealing between model and turntable should be applied.

B.6 Angle of attack

The angle of attack is measured with high precision based on an encoder positioned on the periphery of the turntable with a diameter of 1.604m. The uncertainty in the measurements is approximately 0.01 deg.

Reference

Althaus D (2019): Measurement of Lift and Drag in the Laminar Wind Tunnel, https://www.iag.uni-stuttgart.de/dateien/pdf/laminarwindkanal_messtechniken/althaus_2.pdf, accessed 13 Dec. 2019

Jones B. M. (1936): The measurement of profile drag by the pitot traverse method, ARC RM 1688

Appendix C Standard wind tunnel corrections

The applied corrections are the standard corrections described in Allen & Vincenti (1944) with a second order correction for the solid blockage from Garner (1966).

The corrections are necessary as the tunnel walls confines the flow and changes the flow around the model compared to the situation in open air.

Generally, the corrections adjusts the q_0-term (the dynamic pressure) used for normalizing the coefficients from the value q_0' for the empty tunnel to the actually value in the test section q_0 (which corresponds to the value in free stream). This apparent value is higher than the empty tunnel value due to the speed-up of the flow caused by the blockage from both the model and the wake.

The corrections are based on two dimensional potential flow theory, where the thickness of the airfoil is modelled with a dipole, and the wake with a source and the lift with a vortex. In order to model the walls mirror images are used. See Allen & Vincenti (1944) for details.

In addition to the blockage effects, the interaction between the lift and the tunnel walls introduces a streamline curvature effect that changes the lift and moment measured in the tunnel and the apparent angle of attack (AoA).

Generally, the corrections increases AoA, decreases the lift (i.e. resulting in a lower slope for the lift coefficient curve) and drag coefficients. Depending on the sign of the lift, the moment coefficient is either decreased or increased.

The corrected AoA is:

$$\alpha = \alpha' + \frac{57.3\sigma}{2\pi\beta}(C_l' + 4C_m') \tag{1}$$

Where α' is the turntable AoA in degrees, C_l is the lift coefficient and C_m is the moment coefficient around quarter chord. β is the compressibility factor

$$\beta = \sqrt{1 - (M')^2} \tag{2}$$

Where M is the Mach number.

In the above and following equations an apostrophe (') denotes uncorrected values.

The solid blockage, including second order effects from p 294 Garner (1966) is:

$$\varepsilon_{SB} = \frac{1+\beta^2}{\beta^3}\Lambda\sigma\left[1 + 1.1\left(\frac{c}{t}\right)\left(\frac{\alpha'}{57.3}\right)^2\right] \tag{3}$$

Where the AoA, α', is in degrees, *(t/c)* is the relative thickness of the airfoil, and *c* is the airfoil chord. The two constants σ and Λ (strength of the dipole modelling the thickness) are

$$\sigma = \frac{\pi^2}{48}\left(\frac{c}{h}\right)^2 \tag{4}$$

$$\Lambda = \frac{16}{\pi}\int_0^1 \frac{y_t}{c}\sqrt{\left[1 - C_{p,t}\right]\left[1 + \left(\frac{dy_t}{dx}\right)^2\right]}\, d\left(\frac{x}{c}\right) \tag{5}$$

Where h is the tunnel width, y_t is the y-coordinate of the base profile, i.e. the profile without camber and $C_{p,t}$ is the pressure coefficient for the base profile at 0 deg AoA and incompressible flow. Xfoil (Drela, 1989) is used to determine Λ.
The wake blockage is:

$$\varepsilon_{WB} = \frac{[1 + \beta^2][1 + 0.4(M')^2]}{\beta^2}\tau C_d' \tag{6}$$

Where τ is

$$\tau = \frac{1}{4}\left(\frac{c}{h}\right) \tag{7}$$

The streamline curvature correction is:

$$\varepsilon_{SC} = \frac{\sigma}{\beta^2} \tag{8}$$

Buoyancy correction is used if the drag is based on surface pressures or force balance:

$$\varepsilon_{BC} = \frac{[1 + 0.4(M')^2]}{\beta^3}\Lambda\sigma \tag{9}$$

Combining the different corrections, the total corrections of the coefficients become:

$$C_l = C_l'[1 - \varepsilon_{SC} - \varepsilon_{SB} - \varepsilon_{WB}] \tag{10}$$

$$C_d = C_d'[1 - \varepsilon_{SB} - \varepsilon_{BC} - \varepsilon_{WB}] \tag{11}$$

$$C_{m,c/4} = C_{m,c/4}'[1 - \varepsilon_{SB} - \varepsilon_{WB}] + \frac{\varepsilon_{SC}}{4}C_l' \tag{12}$$

Where the buoyancy correction, ε_{BC}, in the drag correction is only included for drag based on surface pressures or the force balance.

C.1 Tunnel correction constants

Table C. 1 gives the values for the constants used in the corrections.

Table C. 1:Constants for the wind tunnel corrections

Airfoil	Λ	σ	τ
NACA63-418	0.411	0.0228	0.0833

Reference

Allen JH and Vincenti GW (1944): Wall Interference in a Two-Dimensioanl-Flow Wind Tunnel, With Consideration of the Effect of Compressibility, NACA-TR-782.

Drela M (1989): XFOIL: an analysis and design system for low Reynolds number airfoils. In: Conference on Low Reynolds Number Airfoil Aerodynamics, University of Notre Dame.

Garner HC (ed.) (1966): Subsonic Wind Tunnel Corrections, AGARDograph 109

Appendix D Pressure Orifices Coordinates

Table D. 1: NACA63-418

x/c	y/c
0.98006	0.00097
0.96005	0.00197
0.94002	0.00211
0.92000	0.00141
0.90000	0.00013
0.85976	-0.00347
0.81963	-0.00823
0.77960	-0.01386
0.73965	-0.02006
0.69976	-0.02660
0.65988	-0.03324
0.59968	-0.04305
0.58005	-0.04611
0.54006	-0.05201
0.50000	-0.05736
0.49990	-0.05737
0.46014	-0.06193
0.42020	-0.06561
0.38018	-0.06824
0.34010	-0.06959
0.30000	-0.06957
0.27988	-0.06910
0.25977	-0.06832
0.23967	-0.06722
0.21960	-0.06579
0.19955	-0.06401
0.17953	-0.06187
0.13962	-0.05645
0.11976	-0.05308
0.10000	-0.04916
0.09231	-0.04745
0.08464	-0.04563
0.07699	-0.04369
0.06939	-0.04162
0.06182	-0.03939
0.05430	-0.03699
0.04685	-0.03438
0.03947	-0.03155
0.03218	-0.02847

0.02502	-0.02511
0.01813	-0.02118
0.01175	-0.01642
0.00609	-0.01078
0.00197	-0.00388
0.00000	0.00396
0.00194	0.01224
0.00629	0.01953
0.01177	0.02596
0.01804	0.03157
0.02479	0.03656
0.03176	0.04121
0.03892	0.04555
0.04623	0.04960
0.05367	0.05340
0.06121	0.05697
0.06885	0.06033
0.07655	0.06351
0.08432	0.06653
0.09213	0.06939
0.10000	0.07211
0.11948	0.07825
0.13915	0.08368
0.17889	0.09284
0.19891	0.09664
0.21902	0.09994
0.23919	0.10277
0.25942	0.10515
0.27969	0.10709
0.30000	0.10862
0.32001	0.10971
0.34004	0.11038
0.36008	0.11060
0.38012	0.11039
0.40015	0.10977
0.42016	0.10878
0.43350	0.10792
0.44016	0.10743
0.44682	0.10691
0.46014	0.10575
0.47344	0.10445
0.48008	0.10376
0.48673	0.10302
0.50000	0.10146

0.50010	0.10145
0.54042	0.09597
0.58071	0.08952
0.66090	0.07426
0.70083	0.06574
0.74068	0.05682
0.78049	0.04770
0.82029	0.03853
0.86011	0.02951
0.90000	0.02077
0.91424	0.01770
0.92850	0.01472
0.94279	0.01189
0.95711	0.00927
0.97146	0.00679
0.98580	0.00422
1.00000	0.00000